Dual-Source Single-Inductor 0.18-μm CMOS Charger–Supply with Nested Hysteretic and Adaptive On-Time PWM Control

Suhwan Kim and Gabriel A. Rincón-Mora

Georgia Institute of Technology, Atlanta, GA U.S.A.

Abstract: Since fuel cells store more energy and batteries supply more power, fuel cell–battery systems can be smaller than single-source supplies. The 0.18-μm CMOS switched-inductor charger–supply shown, for example, draws constant power from an energy source and supplementary power from a battery to supply a 0.8-V load and recharge the battery with excess power. With 62% – 83% efficiency across 0.1 – 8-mA and ±40 mV of worst-case ripple, the system requires 65% less space than a single source occupies.

A major challenge with emerging microsensors, biomedical implants, and other portable devices is operational life, because tiny batteries exhaust quickly. And even though 1-g fuel cells store 5× – 10× more energy than 1-g Li Ions, fuel cells supply 10× – 20× less power [1]. This means fuel cells last longer with light loads and Li Ions output more power across shorter periods. So when peak power is far greater than average power, which is typically the case in wireless sensors, for example, a hybrid can occupy less space than one source [1]. Still, managing a fuel cell and a battery to supply a load and recharge the battery, which also acts as an output, with little space is difficult. Switched-inductor circuits are appealing in this respect because they draw and supply more power with higher efficiency than their linear and switched-capacitor counterparts. Inductors, however, are bulky, so microsystems can only rely on one inductor [2–3]. Today, most single-inductor multiple-output systems derive power from one source [3–4, 6], so the fuel cell and battery require considerable space. And those that use two sources [5] do not manage how much power each should supply across loading conditions, and while [2] does, the efficiency of [2] is low. The advantage of the prototyped 0.18-μm CMOS dual-source single-inductor system built and presented here is less overall volume because it incorporates the functional intelligence of [2] with much higher efficiency.

I. Operational Modes

Because the 1.1 – 1.3-V energy source v_{ES} supplies more energy when delivering constant power, the prototyped system in Figs. 1 and 7 draws constant power P_{ES} from v_{ES} and supplementary power from the 1.8-V power source v_{PS} to supply a 8-

mA, 0.8-V load. When P_{ES} exceeds the needs of the load in P_O, the system uses the excess to recharge v_{PS}. Since the hybrid supply uses and switches a 50-μH 6 × 6 × 2-mm^3 inductor L_O to transfer power between v_{ES}, v_{PS}, and the output v_O, the purpose of capacitors C_{IN} and C_O is to suppress switching noise in v_{ES} and v_O. This way, when P_{ES} surpasses P_O, C_O's voltage and v_O rise above the reference V_{REF} to such an extent that comparator CP_M trips to push the system into the light-load region. CP_M pulls the system back into the heavy-mode region when the opposite happens, when P_O exceeds P_{ES} to pull v_O below CP_M's lower hysteretic threshold.

II. Light-load Region

When lightly loaded, comparator CP_{LT} regulates v_O about V_{REF} and L_O conducts in discontinuous conduction mode (DCM) across the period of the 40-kHz clock f_{CLK}. More specifically, CP_{LT} senses v_O to determine which output: v_O or v_{PS}, should receive L_O's energy. For this, S_{ES} and S_E in Figs. 1 and 2 first energize L_O from v_{ES} to ground across τ_{EN}'s 1.2-μs pulse width to raise L_O's current i_L from zero to 30 mA. Afterwards, S_{ES} and S_E open and $v_{E.OFF}$ in Fig. 2 rises to close S_{DE} and either S_O or S_{PCHG}. If comparator CP_{LT} senses v_O is below V_{REF} by 10 mV, S_O drains L_O into v_O; otherwise, S_{PCHG} depletes L_O into v_{PS}. Comparators CP_{IOZ} and CP_{IPZ} then disengage S_O and S_{PCHG} together with S_{DE} when S_O's and S_{PCHG}'s current i_L nears zero, when L_O is close to empty, which happens at 2.7 and 27 μs in Fig. 2. All switches remain open after that until f_{CLK} initiates another cycle.

Luckily, CP_{LT}, CP_{IOZ}, and CP_{IPZ} need not operate across f_{CLK}'s entire 25-μs period. CP_{LT}, for one, needs to sense v_O only at the end of τ_{EN}'s 1.2-μs pulse width. This is why f_{CLK} in Fig. 2 engages CP_{LT} a short delay τ_D after τ_{EN} rises, to be ready by the end of τ_{EN}, and disengages CP_{LT} another short delay τ_D after τ_{EN} falls. Similarly, CP_{IOZ} and CP_{IPZ} must sense only when S_O and S_{PCHG} conduct i_L, so CP_{LT}'s output v_{LT} enables CP_{IOZ} and CP_{IPZ} and CP_{IOZ}'s and CP_{IPZ}'s flip flops disable them after they detect i_L nears zero. Duty-cycling CP_{LT}, CP_{IOZ}, and CP_{IPZ} this way reduces their power consumption by 90%.

II. Heavy-load Region

When heavily loaded, L_O draws one energy packet from v_{ES} and one variable packet from v_{PS} that transconductor G_{HV} in Figs. 1 and 3 controls when regulating v_O about V_{REF}. As with light loads, L_O stops conducting after that until f_{CLK} starts another cycle. Comparator CP_{HV} compares G_{HV}'s slow-moving output v_G against a triangular saw-tooth voltage v_{SAW} to pulse-width modulate (PWM) how long L_O energizes from v_{PS}. For all this, like before, S_{ES} and S_E first energize L_O from v_{ES} to ground across τ_{EN}'s 1.2-μs pulse width to raise L_O's current i_L from zero to 30 mA. Afterwards, S_{ES} and S_E open and S_{DE}

and S_O close to drain L_O into v_O. S_{DE} then opens and, if G_{HV} senses that v_O still needs power, v_{SAW} starts ramping and S_{PE} closes to energize L_O from v_{PS} to v_O. When v_{SAW} falls below G_{HV}'s v_G, S_{PE} opens and S_{DE} closes to deplete L_O into v_O. S_{DE} and S_O then open when CP_{IOZ} in Fig. 3 senses that L_O's i_L is nearly zero, after which point all other switches remain open until the next f_{CLK} cycle.

III. Measured Performance

As Fig. 4 illustrates, v_O ripples at ±2.5 mV when lightly loaded with 0.1 mA and ±40 mV when heavily loaded with 8 mA. The ripple is higher at 8 mA because v_{ES} and v_{PS} deliver power early in the period and the load slews C_O afterwards, when disconnected from L_O. Since CP_M determines which mode to assert in hysteretic fashion, the system transitions through modes across rising and falling 0.1 – 8-mA load dumps quickly and without ringing oscillations. When the load is light at 0.1 – 1 mA, the fraction of v_{ES} power that v_O and v_{PS} receive is 62% – 73%, as Fig. 5 shows. And the fraction of power v_O receives from v_{ES} and v_{PS} when heavily loaded with 1 – 8 mA is 62% – 84%. Power-conversion efficiency η_C bottoms when the system transitions across 1 mA and peaks to 73% under hysteretic control below 1 mA and 84% under PWM control above 1 mA. η_C peaks at two points because switches are smaller in light mode than in heavy mode, so conduction and gate-drive losses balance at two load levels.

IV. Conclusions

The key feature of the single-inductor 0.18-μm CMOS charge–supply prototyped and validated here is managing two complementary sources with 62% – 84% power-conversion efficiency. For this, the system duty-cycles circuit blocks, operates the inductor in discontinuous conduction mode, and employs hysteretic and PWM control schemes to regulate the output in and across light and heavy modes. The challenge with single-source systems when lightly loaded over extended periods and pulsed periodically with heavy loads, as in the case of wireless sensors, is that oversizing a fuel cell to output more power or a Li Ion to last longer demands more space than an efficient hybrid. To sustain a 0.1 – 10-mW load for one month, for example, [4] and [6] in the table of Fig. 6 require a 1-g fuel cell to supply 10 mW or a 0.45-g or 0.43-g Li Ion to last one month. And because [5] cannot adjust how much power each source should supply according to the load, [5] similarly needs a 1-g fuel cell or a 0.43-g Li Ion. [2] can manage a fuel cell and a Li Ion according to the load, but the cost of intelligence, robustness, and accuracy is unfortunately efficiency, so this hybrid system demands more space than [4–6].

The dual-source single-inductor charger–supply presented here, however, requires a 0.1-g fuel cell and a 0.05-g Li Ion, which combined is 65% less weight at 0.15 g than that of the smallest counterpart.

Acknowledgement

The authors thank Pooya Forghani, Paul Emerson, and Texas Instruments for their support and for fabricating the prototyped IC.

References

[1] M. Chen, J.P. Vogt, and G.A. Rincón-Mora, "Design Methodology of a Hybrid Micro-Scale Fuel Cell-Thin-Film Lithium Ion Source," *IEEE International Midwest Symp. Circuits and Systems*, pp. 674-677, Aug. 2007.

[2] S. Kim and G.A. Rincón-Mora, "Single-Inductor Dual-Input Dual-Output Buck-Boost Fuel Cell-Li Ion Charging DC-DC Converter," *IEEE International Solid-State Circuits Conference (ISSCC)*, pp. 444-445, San Francisco, CA, Feb. 2009.

[3] D. Ma, W.H. Ki, C.Y. Tsui, and P.K.T. Mok, "Single-Inductor Multiple-Output Switching Converters with Time-Multiplexing Control in Discontinuous Conduction Mode," *IEEE J. Solid-State Circuits*, vol. 38, no. 1, pp. 89-100, Jan. 2003.

[4] M.H. Huang and K.H. Chen, "Single-Inductor Multi-Output (SIMO) DC-DC Converters with High Light-Load Efficiency and Minimized Cross-Regulation for Portable Devices," *IEEE J. Solid-State Circuits*, vol. 44, no. 4, pp. 1099-1111, Apr. 2009.

[5] K.W.R. Chew, Z. Sun, H. Tang, and L. Siek, "A 400nW Single-Inductor Dual-Input-Tri-Output DC-DC Buck-Boost Converter with Maximum Power Point Tracking for Indoor Photovoltaic Energy Harvesting," *ISSCC Dig. Tech. Papers*, pp.68-69, Feb. 2013.

[6] Y. Qiu, C.V. Liempd, B. Op het Veld, P.G. Blanken, and C.V. Hoof, "5μW-to-10mW Input Power Range Inductive Boost Converter for Indoor Photovoltaic Energy Harvesting with Integrated Maximum Power Point Tracking Algorithm," *ISSCC Dig. Tech. Papers,* pp. 118-120, Feb. 2011.

Captions:

Figure 1: Dual-source single-inductor 0.18-μm CMOS charger–supply.

Figure 2: Light-load circuit and related waveforms.

Figure 3. Heavy-load circuit and related waveforms.

Figure 4: Rising and falling load-dump responses and output regulation across operating modes.

Figure 5: Simulated and measured power-conversion efficiency.

Figure 6: Performance summary and comparison with the state of the art.

Figure 7: Fabricated die and experimental printed-circuit board.

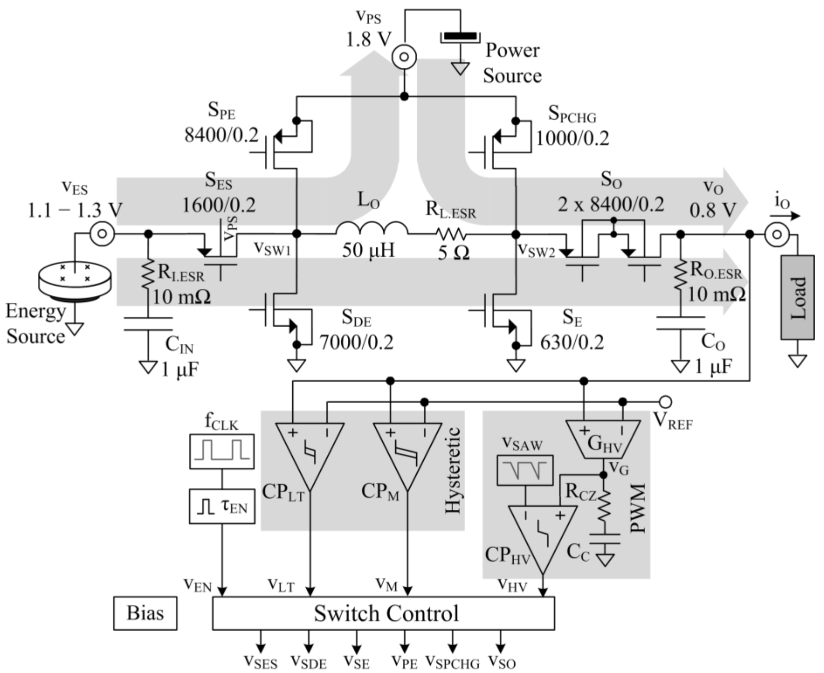

Figure 1: Dual-source single-inductor 0.18-µm CMOS charger–supply.

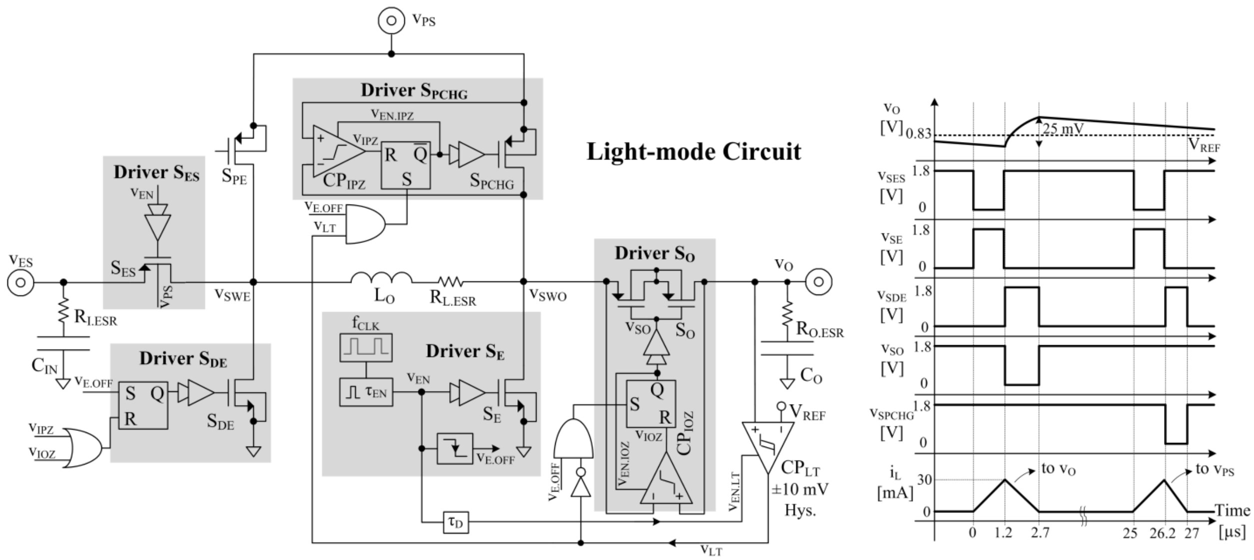

Figure 2: Light-load circuit and related waveforms.

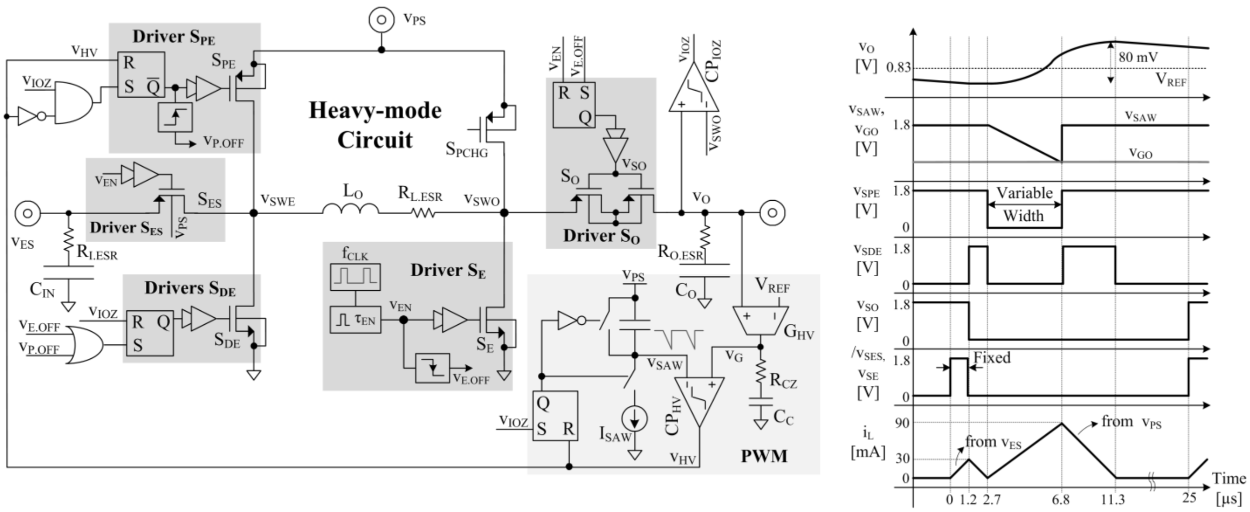

Figure 3: Heavy-load circuit and related waveforms.

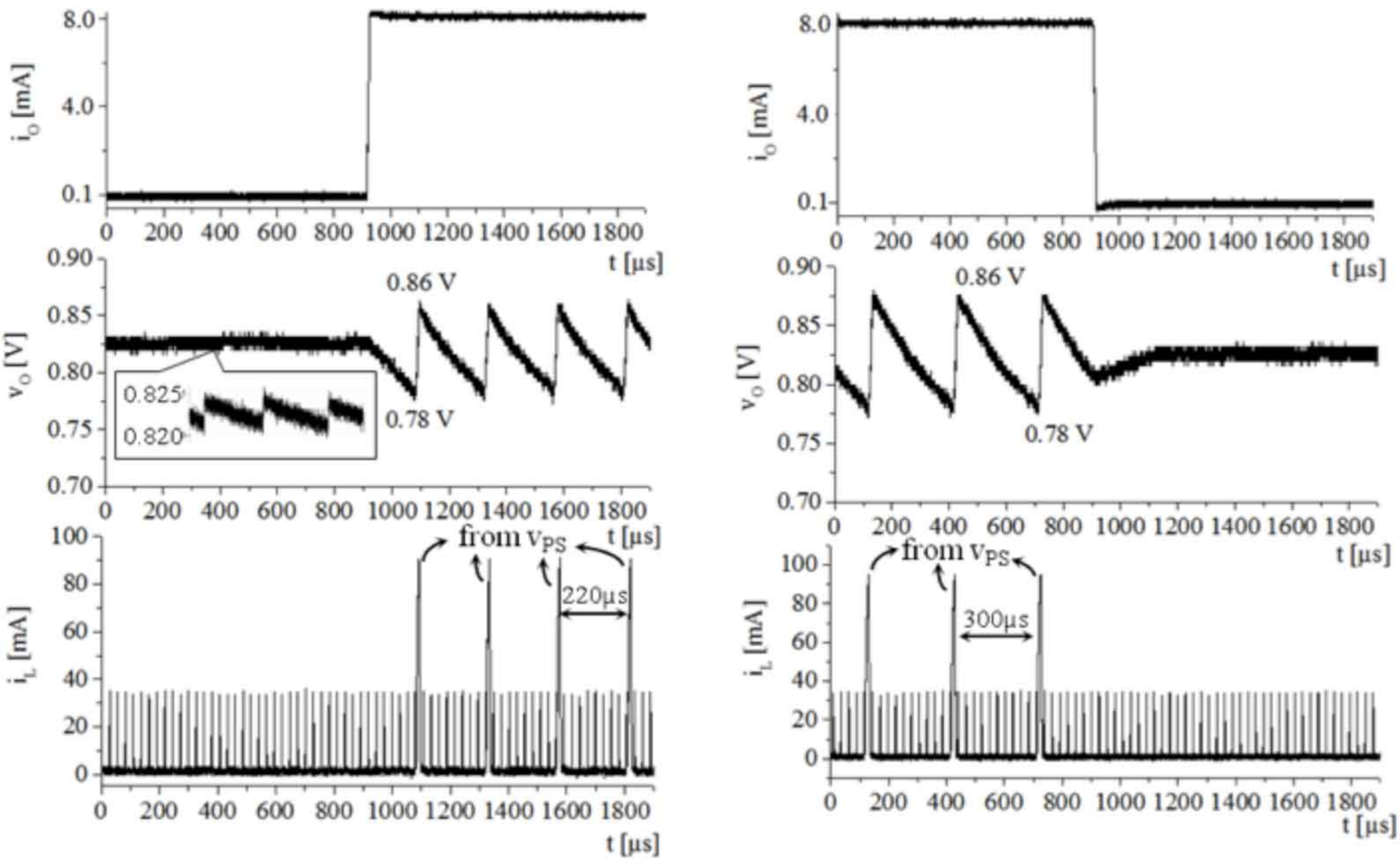

Figure 4: Rising and falling load-dump responses and output regulation across operating modes.

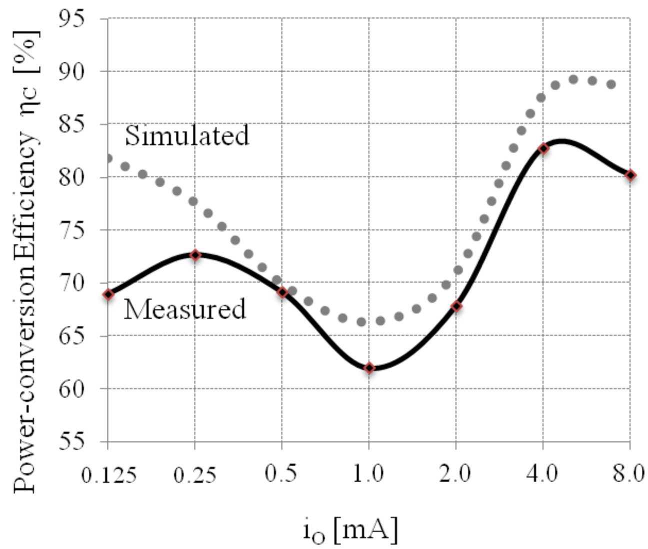

Figure 5: Simulated and measured power-conversion efficiency.

	[2] ISSCC 09	[4] JSSC 09	[5] ISSCC 13	[6] ISSCC 11	This work
Topology	SIDIDO Buck-Boost	SIMO Buck-Boost	SIDITO Buck-Boost	SISO Boost	SIDIDO Buck-Boost
Efficiency @ 0.1 mW / Peak	4% / 32%	80% / 93%	83% / 83%	83% / 87%	70% / 83%
Output Voltage	1.0	1.25	1, 1.8, 3	1.5, 3, 5	0.8
Load Dump/Filter cap	60 mV / 0.1 μF	25 mV / 33 μF	N/A	N/A	30 mV / 1 μF
Load Range	0 - 1 mW	0 - 125 mW	0 - 10 mW	0 - 10 mW	0 - 10 mW
Inductor	150 μH	10 μH	N/A	1000 μH	50 μH
Process	0.5 μm	0.25 μm	0.18 μm	0.25 μm	0.18 μm
Required sources' volume to supply 0.1 - 10 mW's loads for 1 month	1.8-g DMFC Or 9.1-g Li Ion	1-g DMFC Or 0.45-g Li Ion	1-g DMFC Or 0.43-g Li Ion	1-g DMFC Or 0.43-g Li Ion	0.1-g DMFC + 0.05-g Li Ion Tot. 0.15 g

Figure 6: Performance summary and comparison with the state of the art.

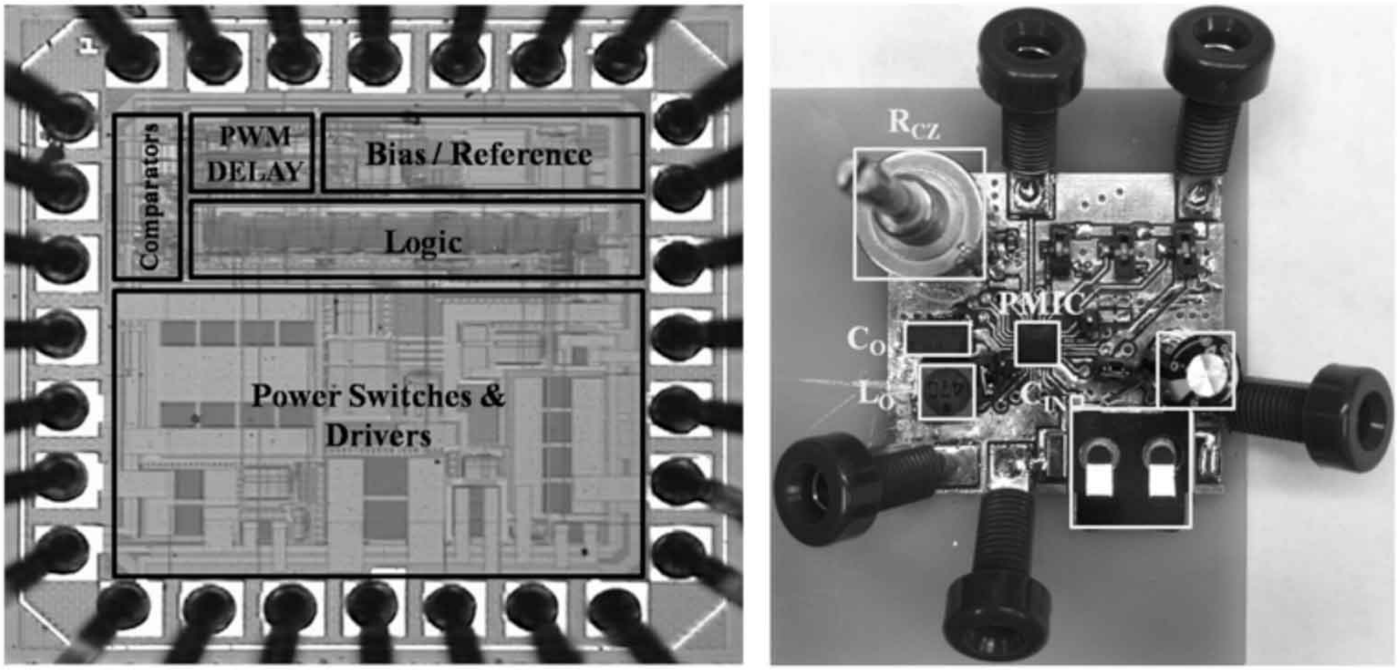

Figure 7: Fabricated die and experimental printed-circuit board.